nature genetics

In situ single-cell analysis identifies heterogeneity for *PIK3CA* mutation and *HER2* amplification in *HER2*-positive breast cancer

Michalina Janiszewska[1–3], Lin Liu[4,5], Vanessa Almendro[1–3], Yanan Kuang[1,6], Cloud Paweletz[1,6], Rita A Sakr[7], Britta Weigelt[8], Ariella B Hanker[9], Sarat Chandarlapaty[10], Tari A King[7], Jorge S Reis-Filho[8,10], Carlos L Arteaga[9,11], So Yeon Park[12], Franziska Michor[4,5] & Kornelia Polyak[1–3,13,14]

Detection of minor, genetically distinct subpopulations within tumors is a key challenge in cancer genomics. Here we report STAR-FISH (specific-to-allele PCR–FISH), a novel method for the combined detection of single-nucleotide and copy number alterations in single cells in intact archived tissues. Using this method, we assessed the clinical impact of changes in the frequency and topology of *PIK3CA* mutation and *HER2* (*ERBB2*) amplification within HER2-positive breast cancer during neoadjuvant therapy. We found that these two genetic events are not always present in the same cells. Chemotherapy selects for *PIK3CA*-mutant cells, a minor subpopulation in nearly all treatment-naive samples, and modulates genetic diversity within tumors. Treatment-associated changes in the spatial distribution of cellular genetic diversity correlated with poor long-term outcome following adjuvant therapy with trastuzumab. Our findings support the use of *in situ* single cell–based methods in cancer genomics and imply that chemotherapy before HER2-targeted therapy may promote treatment resistance.

Cancer is a genetic disease, and the identification of somatic genetic alterations in tumors thus has been the focus of clinical oncology. Cancer genome sequencing studies have traditionally been performed on bulk tumor samples, limiting their ability to detect minor subclones, which commonly drive therapy resistance[1,2]. Sequencing of bulk tumor samples also cannot accurately predict which mutations are present in the same or in different cells. Sequencing of single cancer cells overcomes these limitations[3,4] but is currently still laborious, expensive and prone to error as a result of the inefficiencies of whole-genome amplification; it is thus not yet suitable for the analysis of large patient cohorts. We have developed a novel methodology, termed STAR-FISH, based on the combination of *in situ* PCR[5–7] and FISH[8–10] to enable the simultaneous detection of point mutations and copy number variations at the single-cell level in intact formalin-fixed, paraffin-embedded tissue samples.

We designed STAR-FISH for several commonly mutated genes in breast cancer, focusing on clinically relevant mutational hotspots. *PIK3CA* is one of the most commonly mutated genes in breast cancer[11]. Mutations in *PIK3CA*[12], predominantly occurring at two hotspots (p.Glu542Lys (c.1624G>A) and p.His1047Arg (c.3140A>G)), are present in about 20% of all breast tumors and in up to 40% of cancers in the HER2-positive subtype. The phosphoinositide 3-kinase (PI3K)-AKT pathway has been identified as a major determinant of resistance to trastuzumab, an antibody targeting HER2 (also known as ERBB2)[13–19], implying that *PIK3CA* mutation might be used as a predictor of resistance. However, the substantial heterogeneity for *PIK3CA* mutation, both within different regions of the same tumor and between different lesions in the same patient[20,21], make its accurate detection challenging. We applied STAR-FISH to assess changes in intratumoral cellular heterogeneity for *HER2* amplification and the *PIK3CA* mutation encoding p.His1047Arg in a cohort of patients with HER2-positive breast cancer subjected to neoadjuvant chemotherapy followed by adjuvant therapy with trastuzumab and correlated these changes with long-term clinical outcome.

RESULTS

STAR-FISH development and validation

The first step of STAR-FISH is an *in situ* PCR reaction using mismatched primers designed to specifically amplify mutant and wild-type alleles (**Fig. 1a**, **Supplementary Fig. 1a**, **Supplementary Table 1**

[1]Department of Medical Oncology, Dana-Farber Cancer Institute, Boston, Massachusetts, USA. [2]Department of Medicine, Brigham and Women's Hospital, Boston, Massachusetts, USA. [3]Department of Medicine, Harvard Medical School, Boston, Massachusetts, USA. [4]Department of Biostatistics and Computational Biology, Dana-Farber Cancer Institute, Boston, Massachusetts, USA. [5]Department of Biostatistics, Harvard T.H. Chan School of Public Health, Boston, Massachusetts, USA. [6]Belfer Institute of Applied Cancer Science, Dana-Farber Cancer Institute, Boston, Massachusetts, USA. [7]Breast Service, Department of Surgery, Memorial Sloan Kettering Cancer Center, New York, New York, USA. [8]Department of Pathology, Memorial Sloan Kettering Cancer Center, New York, New York, USA. [9]Department of Cancer Biology, Vanderbilt-Ingram Cancer Center, Vanderbilt University, Nashville, Tennessee, USA. [10]Human Oncology and Pathogenesis Program, Memorial Sloan Kettering Cancer Center, New York, New York, USA. [11]Department of Medicine, Breast Cancer Research Program, Vanderbilt-Ingram Cancer Center, Vanderbilt University, Nashville, Tennessee, USA. [12]Department of Pathology, Seoul National University College of Medicine, Seoul, South Korea. [13]Broad Institute, Cambridge, Massachusetts, USA. [14]Harvard Stem Cell Institute, Cambridge, Massachusetts, USA. Correspondence should be addressed to K.P. (kornelia_polyak@dfci.harvard.edu) or F.M. (michor@jimmy.harvard.edu).

Received 8 June; accepted 31 July; published online 24 August 2015; doi:10.1038/ng.3391

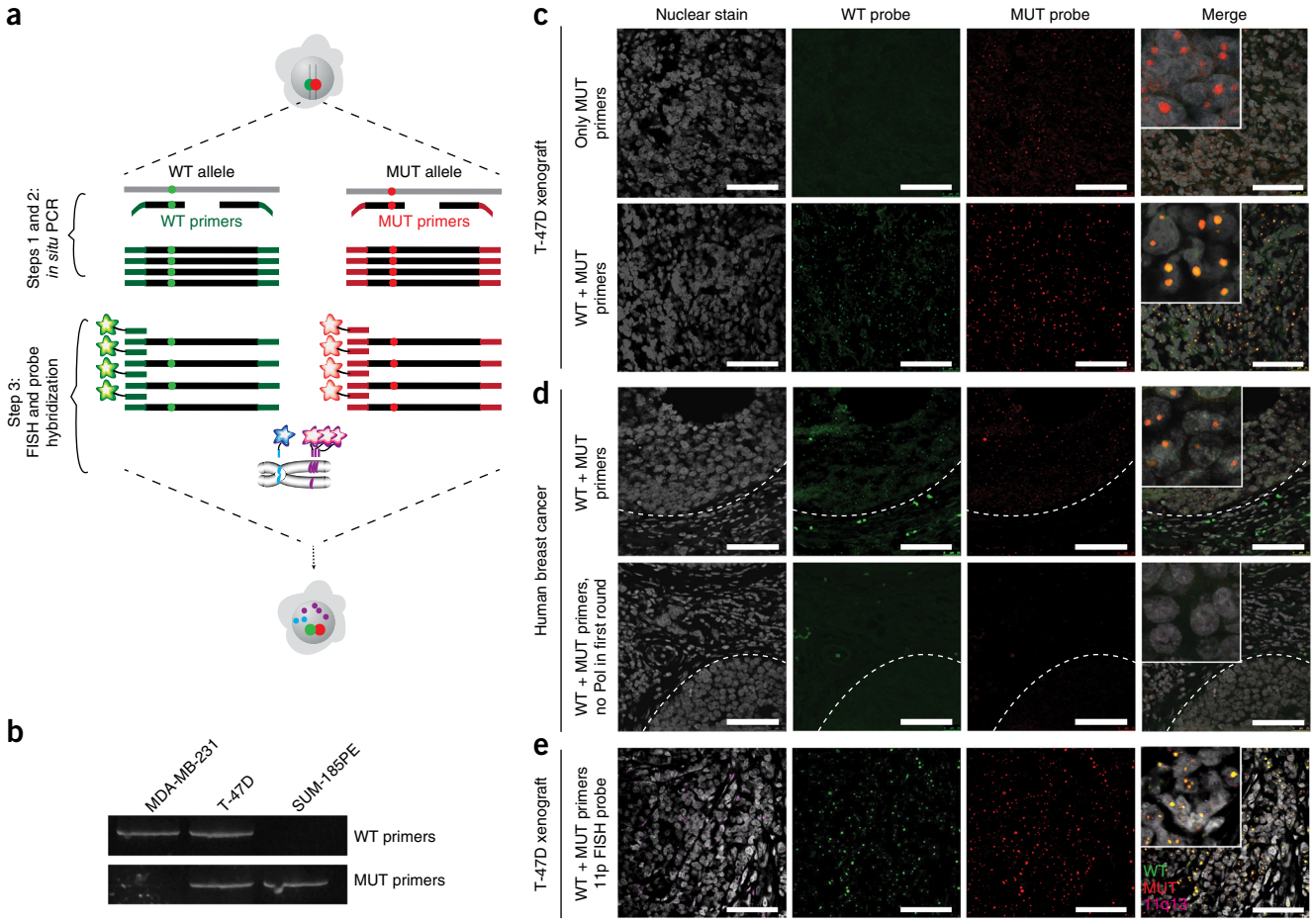

Figure 1 Outline of the STAR-FISH method and its validation. (**a**) Schematic of the STAR-FISH protocol performed on a cell heterozygous for a mutation. In steps 1 and 2, *in situ* PCR with a mixture of primers to the wild-type (WT; green) and mutant (MUT; red) gene is performed. Red and green dots represent the mutation site. In step 3, hybridization of fluorescently labeled probes specific for the wild-type and mutant PCR products is combined with hybridization of BAC (magenta) and CEP (blue) probes for the detection of genomic copy number variation. (**b**) PCR to test the specificity of the primers for the *PIK3CA* His1047 codon using genomic DNA from breast cancer cell lines with known mutation status. MDA-MB-231, *PIK3CA* wild type; T-47D, heterozygous for the *PIK3CA* mutation encoding p.His1047Arg; SUM-185PE, homozygous for the *PIK3CA* mutation encoding p.His1047Arg. (**c**) *In situ* PCR testing the specificity of the primers for wild-type and mutant (p.His1047Arg) *PIK3CA* on T-47D breast cancer cell line xenografts. Top, only primers to the mutant allele were used in the first round of PCR, and both primer sets were used in the second round of PCR. Bottom, primers to both the wild-type and mutant alleles were used in both rounds of PCR. (**d**) *In situ* PCR for wild-type and mutant (p.His1047Arg) *PIK3CA* on a human primary breast tumor sample with known status for the *PIK3CA* mutation encoding p.His1047Arg. Top, the complete *in situ* PCR reaction. Bottom, *in situ* PCR without the polymerase (Pol) in the first round of PCR. The dashed lines show the tumor-stroma border. (**e**) STAR-FISH for wild-type (green) and mutant (His1047Arg; red) *PIK3CA* in combination with FISH with the 11q13x BAC probe (magenta) on a xenograft derived from the T-47D cell line. Scale bars in **c**–**e**, 75 µm; insets are magnified 4.5× from the original images.

and **Supplementary Note**). The primers contain a 5′ overhang constituting a unique sequence not found in the human genome, which serves as a priming site in the second round of PCR. The use of a few amplification cycles in the first round of PCR and 30 amplification cycles in the second round of PCR ensures proper amplification of the product with high specificity. PCR products are visualized by hybridization with fluorescently labeled probe complementary to the 5′ overhang (**Fig. 1a**). The specificity of the primers for the *PIK3CA* mutation encoding p.His1047Arg was first evaluated by PCR using genomic DNA isolated from human breast cancer cell lines with known *PIK3CA* mutation status (**Fig. 1b**). The sensitivity of the assay was tested by performing PCR on defined mixtures of DNA from the MDA-MB-231 (*PIK3CA* wild type) and SUM-185PE (homozygous for the *PIK3CA* mutation encoding p.His1047Arg) cell lines (**Supplementary Figs. 1b** and **2**). Primers for the second round of PCR were tested in the same manner (data not shown). We also developed PCR assays for two other commonly occurring mutations in breast cancer, *PIK3CA* mutation encoding p.Glu542Lys and *TP53* mutation encoding p.Arg175His (**Supplementary Fig. 1c**,**d**).

Next, we performed *in situ* PCR on formalin-fixed, paraffin-embedded tissue slides of xenografts derived from the MDA-MB-231 and T-47D breast cancer cell lines in mice (**Fig. 1c** and **Supplementary Fig. 1e**) followed by testing of primary human breast tumors with known status for the *PIK3CA* mutation encoding p.His1047Arg (**Fig. 1d**). Signal for wild-type and mutant *PIK3CA* was robustly detected in cancer cells, whereas only wild-type signal was visible in surrounding stromal cells (**Fig. 1d**). The false discovery rate (FDR) for *PIK3CA* mutation detection was equal to 1 in 976 cells (FDR = 0.001), on the basis of analysis of xenografts derived from the MDA-MB-231 cell line (*PIK3CA* wild type). No signal was detected when the polymerase was omitted in the first round of PCR, confirming the specificity of the *in situ* PCR step (**Fig. 1d**). Similarly, we performed *in situ* PCR for

the *PIK3CA* mutation encoding p.Glu542Lys and the *TP53* mutation encoding p.Arg175His on BT-483 cells in HistoGel and xenografts derived from AU565 cells, respectively, which are known to contain these mutations (**Supplementary Fig. 1f**,**g**).

To validate the sensitivity and specificity of the *PIK3CA in situ* PCR, we compared it to three independent methods: FACS, immunofluorescence and mass spectrometry[22]. For the comparisons with FACS and immunofluorescence, we used xenografts derived from defined mixtures of wild-type and mutant cell lines expressing fluorescent tags. The mutant cell fraction determined by STAR-FISH was in accordance with the FACS and immunofluorescence results, and the variance between replicates was not significantly different between the various methods (**Supplementary Fig. 3a–d**). For comparison with mass spectrometry, we performed *in situ* PCR for the *PIK3CA* mutation encoding p.His1047Arg on a cohort of breast tumors previously genotyped for this mutation by Sequenom MassARRAY[23,24]. We observed a strong correlation (linear regression $y = 1.013x$, $P < 0.0001$; $R^2 = 0.9037$, $P < 0.0001$) between the two methods (**Supplementary Fig. 4a–c**). Interestingly, even in samples where MassARRAY did not detect any mutant *PIK3CA* alleles, with STAR-FISH, we identified rare mutant cells below a frequency of 8%.

Lastly, we combined *in situ* PCR for the *PIK3CA* mutation encoding p.His1047Arg with FISH for a chromosomal region commonly gained in breast cancer and validated this method on a xenograft derived from the T-47D cell line, which is heterozygous for the *PIK3CA* mutation encoding p.His1047Arg and has an amplification at 11q13 (**Fig. 1e**). We were able to detect clear signals for 11q13 amplification and both wild-type and mutant *PIK3CA* alleles in individual cancer cells. These results confirmed the high specificity and sensitivity of the STAR-FISH assay for the *in situ* detection of single-nucleotide mutations in combination with genomic copy number variation.

STAR-FISH analysis of HER2-positive breast tumor samples

We applied STAR-FISH for the analysis of *PIK3CA* mutation encoding p.His1047Arg and *HER2* amplification status in a cohort of 22 patients with HER2-positive breast cancer undergoing neoadjuvant chemotherapy followed by adjuvant treatment with trastuzumab (**Supplementary Fig. 5** and **Supplementary Table 2**). For each patient, we analyzed a treatment-naive biopsy sample and surgical excision of the residual tumor after neoadjuvant treatment. In each tissue sample, we evaluated 3–5 distinct areas of the tumor to account for regional heterogeneity. Using STAR-FISH, we quantified copy numbers for *HER2* and chromosome 17 centromeric (CEP17) probes and *PIK3CA* wild-type and mutant signal in individual nuclei (on average, 289 nuclei per area; **Fig. 2a**,**b**). Cells with nuclei having <200 pixels in the images were excluded as they likely correspond to infiltrating leukocytes. *HER2* amplification was defined using *HER2*/CEP17 ratio ≥2.0 as the cutoff[25]. To facilitate further statistical and intratumoral diversity analyses based on these single-cell measurements, each cell with evaluable signal was assigned to one of the following categories: WT, a cell with wild-type *PIK3CA* signal and no *HER2* amplification; WT + AMP, a cell with wild-type *PIK3CA* signal and *HER2* amplification; MUT, a cell with mutant *PIK3CA* signal and no *HER2* amplification; MUT + AMP, a cell with mutant *PIK3CA* signal and *HER2* amplification; AMP, a cell with no *PIK3CA* signal and *HER2* amplification (**Fig. 2c** and **Supplementary Table 3**). A subset of cells with no detectable signal for any of the four probes analyzed (NA) and cells with no *PIK3CA* signal and no *HER2* amplification (HER2noAmp) were excluded from further analyses, as these cells likely represent non-specific technical outliers (**Supplementary Fig. 6**, **Supplementary Table 4** and **Supplementary Note**).

Analyzing the frequency of these cell types in all cases demonstrated that the majority of the untreated tumors were composed of cells with *HER2* amplification and wild-type *PIK3CA*, with very small fractions of cells with mutant *PIK3CA* (**Fig. 3a** and **Supplementary Figs. 7** and **8a**). In contrast, the residual tumors after neoadjuvant therapy showed a dramatic increase in the relative frequency of *PIK3CA*-mutant cells and a less pronounced decrease in the fraction of cells with *HER2* amplification (**Fig. 3a** and **Supplementary Figs. 7** and **8a**,**b**). These results demonstrate that cells with *PIK3CA* mutation exist in HER2-positive tumors before therapy but represent a minor population. The high sensitivity of STAR-FISH is reflected in our ability to detect these cells in almost all (20/22) of the untreated biopsy samples. In The Cancer Genome Atlas (TCGA) breast cancer study[12], *PIK3CA* mutation encoding p.His1047Arg was only detected in 17% of HER2-positive tumors. This seeming discrepancy can be explained by the fact that, in 17 of 22 (77.3%) cases, the cells with *PIK3CA* mutation

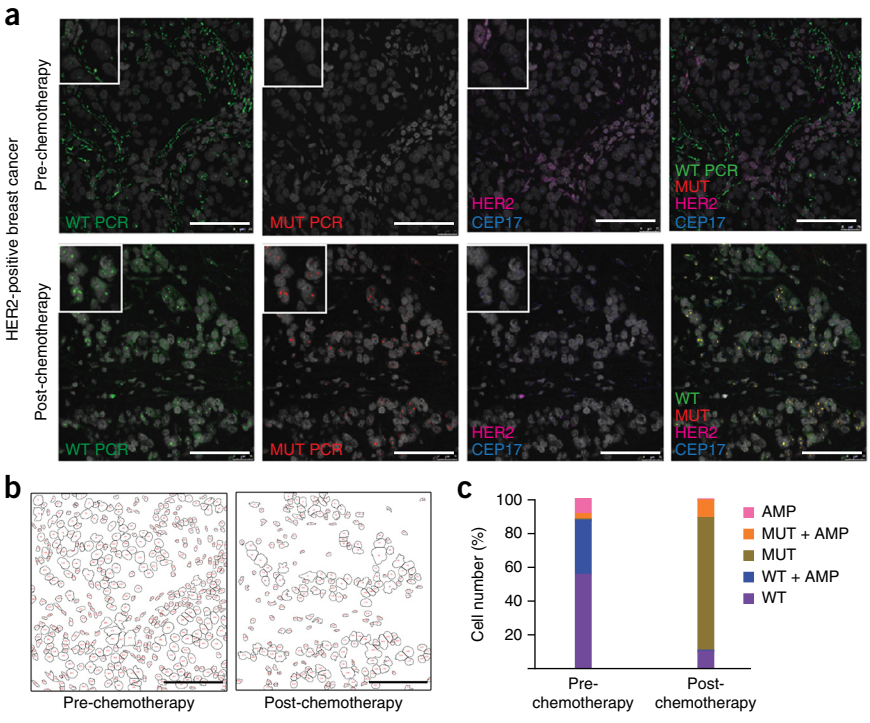

Figure 2 STAR-FISH analysis of breast cancer. (**a**) STAR-FISH performed on a HER2-positive tumor before and after neoadjuvant chemotherapy. Green, wild-type *PIK3CA*; red, mutant *PIK3CA*; blue, CEP17; magenta, *HER2*; gray, nuclear stain (To-Pro-3). (**b**) Automated quantification of STAR-FISH signal in single cells. Images represent tumor topology before and after chemotherapy based on computational segmentation of confocal images of the nuclei. Each nuclear outline present was used as a region of interest (single nucleus) in which STAR-FISH signals were quantified. Scale bars in **a** and **b**, 75 µm; insets in **a** are magnified 1.9× from the original images (**c**) The graph depicts the frequency of cells in each of the five defined cell categories ('species') before and after treatment.

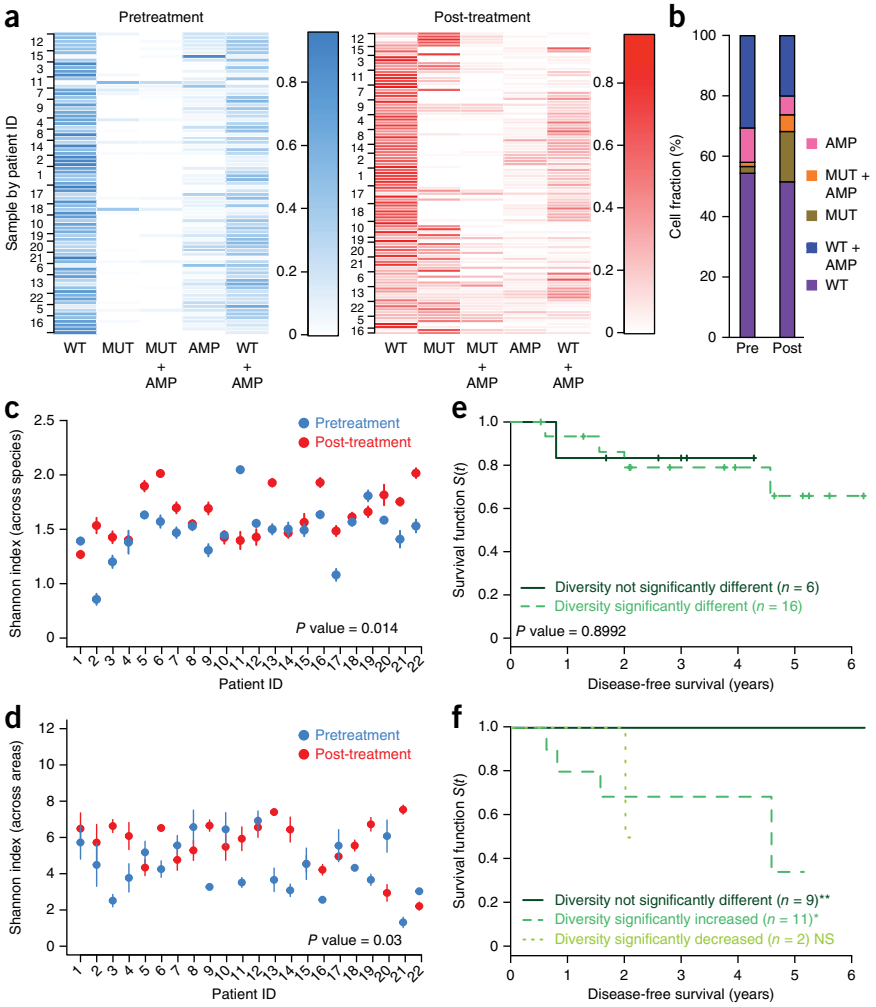

Figure 3 Changes in intratumoral heterogeneity and patient outcomes. (**a**) Frequency of each cell type before and after treatment. Rows show single areas of a tumor (numbers are patient IDs). Columns show cell types (**Supplementary Table 3**). Samples are clustered on the basis of the frequencies of the cell types in the pretreatment samples. Color intensity indicates frequency. (**b**) Summary of cell type frequencies in all patients combined before (Pre) and after (Post) therapy. The graph depicts the mean percentage of each cell type in all areas and samples combined. (**c**,**d**) Shannon index of diversity based on counts of the five cell types combining all areas in each sample in an across-species comparison (**c**) and across different areas of the same tumor in an across-area comparison (**d**). Confidence intervals were defined by nonparametric bootstrap resampling. The global difference in diversity before and after treatment for all patients was calculated using the paired Wilcoxon signed-rank test. Error bars represent two times the standard error obtained from 1,000 bootstrap samples. (**e**,**f**) Changes in diversity and clinical outcome. Associations between changes in cellular diversity after chemotherapy across species (**e**) and across areas (**f**). Patients are grouped on the basis of changes in diversity after treatment. $^{**}P = 0.0178$, $^{*}P = 0.0596$; NS, (not significant) $P = 0.359$. *P* values were calculated by log-rank test.

encoding p.His1047Arg constituted less than 5% of all cells in the tumor and therefore would not be detected by bulk tumor sequencing at the depths of coverage attained in the TCGA breast cancer study. To validate our STAR-FISH results by an independent, highly sensitive mutation detection method, we performed droplet digital PCR[26,27] using DNA extracted from formalin-fixed, paraffin-embedded slides adjacent to the ones used for STAR-FISH (**Supplementary Fig. 9a–d** and **Supplementary Note**). *PIK3CA*-mutant cell detection with the two methods was highly concordant for samples with more than 20% tumor cell content (linear regression $y = 0.6835x$, $P < 0.0001$; correlation $R^2 = 0.901$, $P = 0.0003$). These results confirm that STAR-FISH allows for the detection of rare mutant cells with high specificity (FDR = 0.001), which is critical for the identification of probable resistance-conferring mechanisms.

Our single-cell analysis of the frequency of cells with *HER2* amplification by STAR-FISH found substantial heterogeneity and changes due to treatment, in line with the results of previous studies[28–39]. In pretreatment samples, only 32.5 ± 18% of all cells contained *HER2* amplification, and this frequency decreased to an average of 23.5 ± 23.4% after neoadjuvant therapy, with considerable variation among patients. Assuming that the heterogeneity of the primary tumor is reflective of that of the disseminated cancer cells targeted by adjuvant therapy, the decrease in the frequency of *HER2*-amplified cells after neoadjuvant therapy may contribute to the suboptimal efficacy of HER2-targeted therapies in some patients. Our results also imply that it would be beneficial to reevaluate tumors after recurrence and design subsequent therapies on the basis of the resulting knowledge.

Changes in intratumoral heterogeneity after chemotherapy

Neoadjuvant chemotherapy appears to enrich for *PIK3CA*-mutant cells, potentially increasing the risk of resistance to subsequent HER2-targeted adjuvant therapies, conferred by the *PIK3CA* mutation but also by enrichment for cells lacking the *HER2* amplicon. Analysis of each individual tumor area (**Fig. 3b**) showed an overall increase in the diversity of cellular subpopulations, as the majority of treatment-naive samples were composed of only three cell populations whereas post-treatment tumors often contained all five cell types (**Supplementary Figs. 7** and **8a**). Moreover, in many samples, there was also substantial variation among different areas of the same tumor, and this variance increased in many cases after chemotherapy (**Supplementary Fig. 7**). These results demonstrate that neoadjuvant chemotherapy changes the relative frequencies of genetically distinct cell populations in treatment-resistant residual tumors and suggest that some of these changes may have an unfavorable impact on the efficacy of subsequent adjuvant HER2-targeted therapies.

To further investigate global changes in intratumoral cellular genetic heterogeneity for *PIK3CA* and *HER2*, we calculated Shannon and Simpson's indices[40] in each sample before and after neoadjuvant treatment. These diversity measures allow for the characterization of each sample by a single value that reflects the relative abundance of cells in each of the five categories. The diversity index was significantly different between samples before and after treatment (**Fig. 3c** and **Supplementary Fig. 8c**,**d**). This significant ($P = 0.014$) shift in diversity was also present when we compared different areas of the same tumor (**Fig. 3d**). These results imply that neoadjuvant treatment influences intratumoral cellular genetic diversity, not only as a result of changes in the frequencies of cell populations but also by increasing regional heterogeneity within tumors.

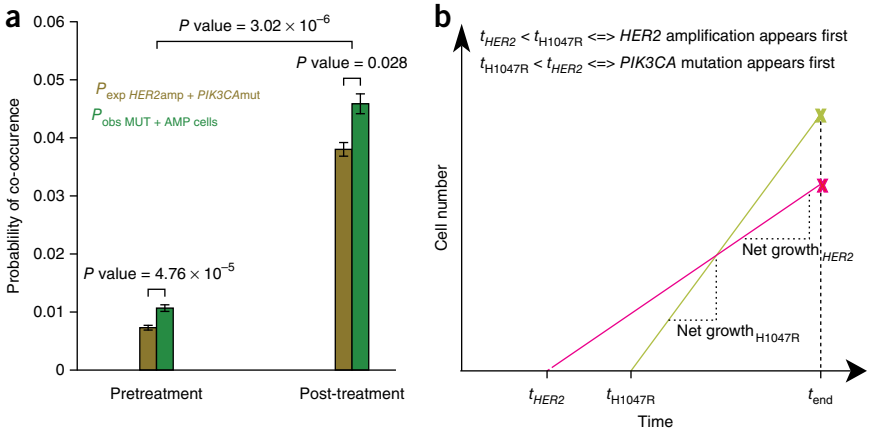

Figure 4 Probable course of tumor evolution based on the co-occurrence of *PIK3CA* mutation and *HER2* amplification. (**a**) Co-occurrence of *PIK3CA* mutation encoding p.His1047Arg and *HER2* amplification in the same cell. The expected probability (P_{exp}) of co-occurrence of the two genetic events is compared with the observed probability (P_{obs}) based on the frequency of MUT + AMP cells. Error bars, s.d. of the expected or observed values divided by the square root of the total number of samples. (**b**) Mathematical model of probable tumor evolution with prediction of the time at which each event arises (t_{HER2} and t_{H1047R}), based on STAR-FISH counts for both events (crosses) at the observation time (t_{end}) and the net growth rates attributed to these events on the basis of published data[42].

Three of the patients received targeted therapy, trastuzumab, in addition to chemotherapy in the neoadjuvant setting (patients 20, 21 and 22). Interestingly, two of these cases had a decrease in diversity after neoadjuvant therapy, suggesting the presence of and selection for a preexisting subpopulation resistant to treatment (**Supplementary Fig. 10**). However, a larger number of samples will be necessary to demonstrate the generality of this finding.

Because *PIK3CA* mutations are thought to be associated with treatment resistance in HER2-positive tumors[15–19] and the changes in intratumoral diversity were in part due to variations in the fraction of *PIK3CA*-mutant cells, we analyzed potential associations between changes in diversity and patient outcome. Interestingly, the difference in cellular diversity between samples before and after neoadjuvant chemotherapy did not affect disease-free survival following adjuvant treatment with trastuzumab (**Fig. 3e**). Similarly, changes in the fraction of *PIK3CA*-mutant cells were not by themselves predictive of recurrence (data not shown). However, when the diversity index was calculated on the basis of the cell type frequencies across different areas of the same tumor, a significant change in diversity was associated with shorter disease-free survival (**Fig. 3f**). Because long-term survival is largely defined by progression to metastatic disease, our results imply a potential role for regional differences in the primary tumor microenvironment in selecting for treatment-resistant cancer cells capable of migration and metastatic dissemination. Surprisingly, both an increase and a decrease in the diversity of cell populations across different areas of the same tumor were associated with shorter disease-free survival (the decrease in diversity did not reach significance, likely owing to the low sample number, $n = 2$). Both patients showing a decrease in diversity across tumor areas after treatment received trastuzumab, a HER2-targeting therapy, in the neoadjuvant setting in addition to receiving it in the adjuvant setting (**Supplementary Fig. 4**). Cell type frequency plots in patients treated with neoadjuvant chemotherapy and trastuzumab (patients 20, 21 and 22) showed that the decrease in post-treatment diversity was due to the high similarity among the areas tested, with all five cell types present in similar proportions. Thus, including trastuzumab in neoadjuvant treatment seems to promote spatial homogeneity, but it does not prevent an increase in post-treatment cellular heterogeneity in patients who do not achieve a complete pathological response. Taken together, these results demonstrate that heterogeneity within primary tumors is an important determinant of long-term clinical outcome and that therapeutic resistance may be associated with changes both in cellular genetic and regional heterogeneity. These results also highlight the need to analyze tumors at the single-cell level *in situ* and the high clinical value of assessing primary tumors before and after neoadjuvant therapy and designing follow-up therapies on the basis of the resulting knowledge.

Co-occurrence of *PIK3CA* mutation and *HER2* amplification

STAR-FISH allows for the detection of genetic alterations in single cells and thus can be used to investigate the co-occurrence of two or more genetic events. The frequency of cells with single or combined genetic alterations can be used to predict the relative order of these changes to decipher the probable course of tumor evolution[41]. Thus, we used our STAR-FISH data to explore the relative order of *HER2* amplification and *PIK3CA* mutation. If the two genetic events arise independently, then the probability of having both events present in the same cell is equal to the product of the probabilities for each individual event (see the Online Methods for details). Thus, if co-occurrence is favored, the probability of having both events is higher than expected by chance. We found that the observed frequency of co-occurrence for *PIK3CA* mutation and *HER2* amplification in the same cell was higher than expected in the samples both before and after treatment (**Fig. 4a**), implying higher fitness for cells with both alterations in comparison to cells with each individually. Co-occurrence of the *PIK3CA* mutation encoding p.His1047Arg with *HER2* amplification within the same tumor has previously been reported[12,39]. However, whether these two genetic alterations are in the same cancer cell or in different subpopulations has not been defined conclusively. Our results indicate that most cells with *PIK3CA* mutation encoding p.His1047Arg do not have *HER2* amplification. Yet, the frequency of cells with both genetic events is significantly ($P = 3.02 \times 10^{-6}$) higher than expected by chance. These results suggest that *PIK3CA* mutation encoding p.His1047Arg and *HER2* amplification are independent genetic events and that cells with both events have a fitness advantage over others. Our results are in line with data in animal models, which show that the combination of *PIK3CA* mutation encoding p.His1047Arg with *HER2* amplification accelerates tumor formation and metastatic progression and confers resistance to HER2-targeted therapies[42].

Model of the relative order of genetic events

Next, we examined the relative order of *PIK3CA* mutation and *HER2* amplification during tumor progression. To determine the time during tumor progression at which these genetic events arose, a mathematical model was constructed on the basis of STAR-FISH–derived numbers of cells with *PIK3CA* mutation and with *HER2* amplification and the cell death and proliferation rates of cells with these genetic alterations,

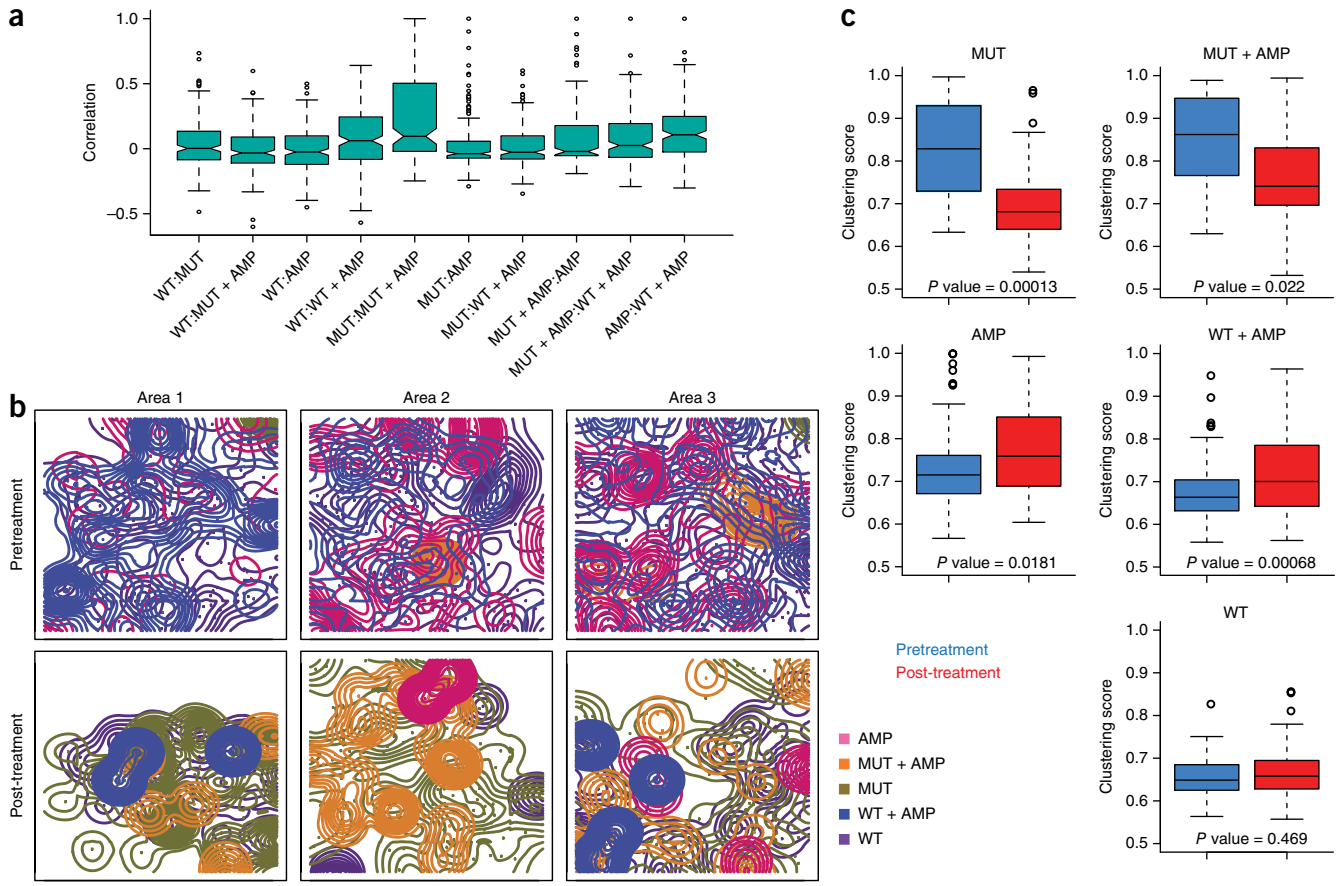

Figure 5 Intratumoral topology. (**a**) Co-occurrence of the indicated cell-type combinations. None of the correlations are significant. The median value is the horizontal bar in the middle of each box. IQR (interquartile range) is defined by the upper and lower edges of each box. Notches are the 95% confidence intervals of the medians. The lower whisker is defined as the maximum between the 25th percentile −1.5 × IQR and the minimum value of the data, and the upper whisker is defined as the minimum between the 75th percentile + 1.5 × IQR and the maximum value of the data. (**b**) Kernel plots depicting the two-dimensional spatial distribution of the indicated cell types in three different regions of the same case before and after treatment. (**c**) Spatial dispersion of different cell types within tumors. Formation of larger clusters in two-dimensional space is indicated by an increase in clustering score, the ratio of between- and within-cluster variation in kernel means: a higher ratio means more clustering, whereas a lower ratio signifies a more random distribution.

individually and in combination, in a transgenic model of HER2-positive breast cancer[42], assuming that the characteristics of human and mouse mammary tumor cells with *PIK3CA* mutation encoding p.His1047Arg and *HER2* amplification are similar (see the Online Methods for details). This model suggested that *HER2* amplification arises first and that *PIK3CA* mutation is acquired at later stages of tumor progression (**Fig. 4b**). Although with the current data it is not possible to predict whether the observed diversity for *PIK3CA* mutation and *HER2* amplification is a result of the parallel evolution of two independent cell populations or diversification at a later stage, our mathematical modeling of the temporal order of events supports the notion that *HER2* amplification is an early event in breast tumor evolution.

Spatial distribution of genetically distinct subpopulations

Our data showing associations between intratumoral diversity across different areas of the same tumor and long-term clinical outcome (**Fig. 3f**) raised the possibility of local microenvironments within primary tumors favoring the expansion of genetically distinct cell populations. To investigate this possibility further, we asked whether different cell types within the tumor were distributed randomly or there was any spatial clustering of cell types. Although we found no significant correlation of the presence of any two individual cell types in the same sample, there was a trend for the co-occurrence of cells with *PIK3CA* mutation alone (MUT) and cells with both *PIK3CA* mutation and *HER2* amplification (MUT +AMP) (**Fig. 5a**).

To further investigate potential relationships between the intratumoral localizations of different cell types, we performed spatial distribution analyses. Kernel density and counts of cell type densities were calculated for each cell type (**Fig. 5b**; see the Online Methods for details). These measurements were used to assess whether cells of a certain type tended to cluster together or be randomly distributed across the investigated area. *k*-means clustering[43] showed that cells with *PIK3CA* mutation, irrespectively of their *HER2* amplification status, tended to form clusters *in situ* (**Fig. 5b**). Cells with wild-type *PIK3CA* and no *HER2* amplification had the lowest clustering score, and this remained unchanged after treatment (**Fig. 5c**). Neoadjuvant therapy seemed to have opposing effects on MUT and MUT + AMP cells in comparison to WT and WT + AMP cells: for cells with *PIK3CA* mutation, the clustering score after treatment was decreased to the level of WT cells (cells were more dispersed after treatment), whereas for AMP and WT + AMP cells the clustering score was increased (cells were less dispersed after treatment). These results suggest that WT cells are most likely non-malignant stromal cells, as their distribution

within tumors neither showed any specific pattern nor was affected by treatment. In contrast, the increased dispersion of cancer cells with *PIK3CA* mutation after treatment implies that these cells might be more migratory. Indeed, *PIK3CA* mutations were shown to increase cell motility[42,44], supporting our hypothesis.

DISCUSSION

The STAR-FISH method we describe here is relatively inexpensive and the results are easy to interpret. It is also much more sensitive than sequencing or mass spectrometry–based[45] methods, as even a single mutant cell can be detected among thousands of cells analyzed with FDR = 0.001. Other methods, such as padlock-probe rolling-circle amplification, can be used to detect mutations *in situ* on the basis of mRNA[46]. However, mRNA levels can be affected by tissue handling, the nature of the mutation (for example, some result in nonsense-mediated decay[47]) and cancer treatment. Thus, methods based on DNA detection such as STAR-FISH are more suited for clinical studies; STAR-FISH in particular is useful for these studies because it utilizes standard formalin-fixed, paraffin-embedded samples that are routinely available. Because intratumoral heterogeneity is one of the main drivers of disease progression and therapy resistance, including STAR-FISH analysis in clinical practice could improve patient stratification and the design of optimal individualized therapies. Owing to its high sensitivity and specificity in detecting mutant cells, STAR-FISH could especially be useful for guiding the design of targeted therapies with known genetic resistance mechanisms. The limitations of STAR-FISH include the need for a priori knowledge of the mutation to be analyzed and the number of fluorophores that can be applied to detect *in situ* PCR products and chromosomal regions. The ability to increase multiplexing by combining STAR-FISH with other detection methods such as FISSEQ[48] or CyTOF-based approaches[49] can transform this novel method into an exceptionally powerful diagnostic pathology assay for single-cell mutation detection and genetic heterogeneity analysis.

In summary, we applied a novel *in situ* technique to assess the clinical impact of changes in intratumoral heterogeneity during neoadjuvant therapy. STAR-FISH detected mutant cells with high sensitivity and did so in intact tissues, enabling mapping of the spatial distribution of subpopulations of cancer cells. Our results show that chemotherapy affects both the frequency and topology of these subpopulations. Changes in diversity across different areas of the same tumor proved to be more significant clinically than changes in overall diversity. This finding suggests that the application of *in situ* techniques might be key for the design of more effective therapies for heterogeneous tumors.

METHODS

Methods and any associated references are available in the online version of the paper.

Note: Any Supplementary Information and Source Data files are available in the online version of the paper.

ACKNOWLEDGMENTS

We thank E. Winer, I. Krop, B. Vogelstein and members of the Polyak and Michor laboratories for their critical reading of the manuscript and useful discussions. We thank A. Marusyk and D. Tabassum for their help with the xenograft assays, R. Witwicki for help with data processing, L. Cameron in the Dana-Farber Cancer Institute Confocal Microscopy center for her technical support, A. Richardson (Dana-Farber Cancer Institute) for providing slides from a human breast tumor with known status for the *PIK3CA* mutation encoding p.His1047Arg, and H. Russness and I. Rye (Oslo University Hospital) for providing the BAC probe for *HER2*. This work was supported by the Dana-Farber Cancer Institute Physical Sciences–Oncology Center (U54CA143798 to F.M.), the European Molecular Biology Organization (EMBO; M.J.), the Swiss National Science Foundation (M.J.), the American Cancer Society (CRP-07-234-06-COUN to C.L.A.) and the Breast Cancer Research Foundation (K.P.).

AUTHOR CONTRIBUTIONS

M.J. developed the STAR-FISH method and performed the experiments and data analyses. V.A. assisted with image acquisition and analyses. L.L. performed mathematical modeling and data analysis. S.Y.P. provided tumor samples. Y.K. and C.P. performed the digital PCR experiment and data analysis. R.A.S., B.W., T.A.K., S.C. and J.S.R.-F. provided patient samples and performed the Sequenom MassARRAY experiment. A.B.H. and C.L.A. provided data and tissues from transgenic models of HER2-positive breast cancer. K.P. and F.M. supervised the study. All authors helped to design the study and write the manuscript.

COMPETING FINANCIAL INTERESTS

The authors declare no competing financial interests.

1. Marusyk, A., Almendro, V. & Polyak, K. Intra-tumour heterogeneity: a looking glass for cancer? *Nat. Rev. Cancer* **12**, 323–334 (2012).
2. Yap, T.A., Gerlinger, M., Futreal, P.A., Pusztai, L. & Swanton, C. Intratumor heterogeneity: seeing the wood for the trees. *Sci. Transl. Med.* **4**, 127ps10 (2012).
3. Navin, N. *et al.* Tumour evolution inferred by single-cell sequencing. *Nature* **472**, 90–94 (2011).
4. Navin, N.E. Cancer genomics: one cell at a time. *Genome Biol.* **15**, 452–464 (2014).
5. Bagasra, O. Protocols for the *in situ* PCR-amplification and detection of mRNA and DNA sequences. *Nat. Protoc.* **2**, 2782–2795 (2007).
6. Ikeda, S., Takabe, K., Inagaki, M., Funakoshi, N. & Suzuki, K. Detection of gene point mutation in paraffin sections using *in situ* loop-mediated isothermal amplification. *Pathol. Int.* **57**, 594–599 (2007).
7. Ebina, M., Martínez, M., Birrer, M.J. & Linnoila, R.I. *In situ* detection of unexpected patterns of mutant *p53* gene expression in non–small cell lung cancers. *Oncogene* **20**, 2579–2586 (2001).
8. Almendro, V. *et al.* Inference of tumor evolution during chemotherapy by computational modeling and *in situ* analysis of genetic and phenotypic cellular diversity. *Cell Rep.* **6**, 514–527 (2014).
9. Almendro, V. *et al.* Genetic and phenotypic diversity in breast tumor metastases. *Cancer Res.* **74**, 1338–1348 (2014).
10. Park, S.Y., Gönen, M., Kim, H.J., Michor, F. & Polyak, K. Cellular and genetic diversity in the progression of *in situ* human breast carcinomas to an invasive phenotype. *J. Clin. Invest.* **120**, 636–644 (2010).
11. Bachman, K.E. *et al.* The *PIK3CA* gene is mutated with high frequency in human breast cancers. *Cancer Biol. Ther.* **3**, 772–775 (2004).
12. Cancer Genome Atlas Network. Comprehensive molecular portraits of human breast tumours. *Nature* **490**, 61–70 (2012).
13. Berns, K. *et al.* A functional genetic approach identifies the PI3K pathway as a major determinant of trastuzumab resistance in breast cancer. *Cancer Cell* **12**, 395–402 (2007).
14. Nagata, Y. *et al.* PTEN activation contributes to tumor inhibition by trastuzumab, and loss of PTEN predicts trastuzumab resistance in patients. *Cancer Cell* **6**, 117–127 (2004).
15. Wang, Y., Liu, Y., Du, Y., Yin, W. & Lu, J. The predictive role of phosphatase and tensin homolog (*PTEN*) loss, phosphoinositol-3 (PI3) kinase (*PIK3CA*) mutation, and PI3K pathway activation in sensitivity to trastuzumab in HER2-positive breast cancer: a meta-analysis. *Curr. Med. Res. Opin.* **29**, 633–642 (2013).
16. Rexer, B.N., Chanthaphaychith, S., Dahlman, K.B. & Arteaga, C.L. Direct inhibition of PI3K in combination with dual HER2 inhibitors is required for optimal antitumor activity in HER2$^+$ breast cancer cells. *Breast Cancer Res.* **16**, R9 (2014).
17. Rexer, B.N. & Arteaga, C.L. Intrinsic and acquired resistance to HER2-targeted therapies in *HER2* gene-amplified breast cancer: mechanisms and clinical implications. *Crit. Rev. Oncog.* **17**, 1–16 (2012).
18. Cizkova, M. *et al. PIK3CA* mutation impact on survival in breast cancer patients and in ERα, PR and ERBB2-based subgroups. *Breast Cancer Res.* **14**, R28 (2012).
19. Cizkova, M. *et al.* Outcome impact of *PIK3CA* mutations in HER2-positive breast cancer patients treated with trastuzumab. *Br. J. Cancer* **108**, 1807–1809 (2013).
20. Deng, G. *et al.* Single cell mutational analysis of *PIK3CA* in circulating tumor cells and metastases in breast cancer reveals heterogeneity, discordance, and mutation persistence in cultured disseminated tumor cells from bone marrow. *BMC Cancer* **14**, 456–467 (2014).
21. Dupont Jensen, J. *et al. PIK3CA* mutations may be discordant between primary and corresponding metastatic disease in breast cancer. *Clin. Cancer Res.* **17**, 667–677 (2011).
22. Jurinke, C., van den Boom, D., Cantor, C.R. & Koster, H. Automated genotyping using the DNA MassArray technology. *Methods Mol. Biol.* **170**, 103–116 (2001).
23. Sakr, R.A. *et al.* PI3K pathway activation in high-grade ductal carcinoma *in situ*—implications for progression to invasive breast carcinoma. *Clin. Cancer Res.* **20**, 2326–2337 (2014).

24. Chandarlapaty, S. *et al.* Frequent mutational activation of the PI3K-AKT pathway in trastuzumab-resistant breast cancer. *Clin. Cancer Res.* **18**, 6784–6791 (2012).
25. Wolff, A.C. *et al.* Recommendations for human epidermal growth factor receptor 2 testing in breast cancer: American Society of Clinical Oncology/College of American Pathologists clinical practice guideline update. *J. Clin. Oncol.* **31**, 3997–4013 (2013).
26. Vogelstein, B. & Kinzler, K.W. Digital PCR. *Proc. Natl. Acad. Sci. USA* **96**, 9236–9241 (1999).
27. Hindson, B.J. *et al.* High-throughput droplet digital PCR system for absolute quantitation of DNA copy number. *Anal. Chem.* **83**, 8604–8610 (2011).
28. Brunelli, M. *et al.* Genotypic intratumoral heterogeneity in breast carcinoma with *HER2/neu* amplification: evaluation according to ASCO/CAP criteria. *Am. J. Clin. Pathol.* **131**, 678–682 (2009).
29. Glöckner, S., Buurman, H., Kleeberger, W., Lehmann, U. & Kreipe, H. Marked intratumoral heterogeneity of c-*myc* and *cyclinD1* but not of c-*erbB2* amplification in breast cancer. *Lab. Invest.* **82**, 1419–1426 (2002).
30. Hanna, W., Nofech-Mozes, S. & Kahn, H.J. Intratumoral heterogeneity of *HER2/neu* in breast cancer—a rare event. *Breast J.* **13**, 122–129 (2007).
31. Vance, G.H. *et al.* Genetic heterogeneity in *HER2* testing in breast cancer: panel summary and guidelines. *Arch. Pathol. Lab. Med.* **133**, 611–612 (2009).
32. Cottu, P.H. *et al.* Intratumoral heterogeneity of HER2/neu expression and its consequences for the management of advanced breast cancer. *Ann. Oncol.* **19**, 595–597 (2008).
33. Lewis, J.T. *et al.* Analysis of intratumoral heterogeneity and amplification status in breast carcinomas with equivocal (2+) HER-2 immunostaining. *Am. J. Clin. Pathol.* **124**, 273–281 (2005).
34. Striebel, J.M., Bhargava, R., Horbinski, C., Surti, U. & Dabbs, D.J. The equivocally amplified *HER2* FISH result on breast core biopsy: indications for further sampling do affect patient management. *Am. J. Clin. Pathol.* **129**, 383–390 (2008).
35. Shin, S.J., Hyjek, E., Early, E. & Knowles, D.M. Intratumoral heterogeneity of HER-2/neu in invasive mammary carcinomas using fluorescence *in-situ* hybridization and tissue microarray. *Int. J. Surg. Pathol.* **14**, 279–284 (2006).
36. Seol, H. *et al.* Intratumoral heterogeneity of *HER2* gene amplification in breast cancer: its clinicopathological significance. *Mod. Pathol.* **25**, 938–948 (2012).
37. Bartlett, A.I. *et al.* Heterogeneous *HER2* gene amplification: impact on patient outcome and a clinically relevant definition. *Am. J. Clin. Pathol.* **136**, 266–274 (2011).
38. Andersson, J., Linderholm, B., Bergh, J. & Elmberger, G. HER-2/neu (c-erbB-2) evaluation in primary breast carcinoma by fluorescent *in situ* hybridization and immunohistochemistry with special focus on intratumor heterogeneity and comparison of invasive and *in situ* components. *Appl. Immunohistochem. Mol. Morphol.* **12**, 14–20 (2004).
39. Ng, C.K. *et al.* Intra-tumor genetic heterogeneity and alternative driver genetic alterations in breast cancers with heterogeneous *HER2* gene amplification. *Genome Biol.* **16**, 107–127 (2015).
40. Magurran, A.E. *Measuring Biological Diversity* (Blackwell, 2004).
41. Martins, F.C. *et al.* Evolutionary pathways in *BRCA1*-associated breast tumors. *Cancer Discov.* **2**, 503–511 (2012).
42. Hanker, A.B. *et al.* Mutant *PIK3CA* accelerates HER2-driven transgenic mammary tumors and induces resistance to combinations of anti-HER2 therapies. *Proc. Natl. Acad. Sci. USA* **110**, 14372–14377 (2013).
43. Hartigan, J.A. & Wong, M. A *K*-means clustering algorithm. *Appl. Stat.* **28**, 100–108 (1979).
44. Samuels, Y. *et al.* Mutant *PIK3CA* promotes cell growth and invasion of human cancer cells. *Cancer Cell* **7**, 561–573 (2005).
45. Thomas, R.K. *et al.* High-throughput oncogene mutation profiling in human cancer. *Nat. Genet.* **39**, 347–351 (2007).
46. Grundberg, I. *et al. In situ* mutation detection and visualization of intratumor heterogeneity for cancer research and diagnostics. *Oncotarget* **4**, 2407–2418 (2013).
47. Chang, Y.F., Imam, J.S. & Wilkinson, M.F. The nonsense-mediated decay RNA surveillance pathway. *Annu. Rev. Biochem.* **76**, 51–74 (2007).
48. Lee, J.H. *et al.* Highly multiplexed subcellular RNA sequencing *in situ*. *Science* **343**, 1360–1363 (2014).
49. Giesen, C. *et al.* Highly multiplexed imaging of tumor tissues with subcellular resolution by mass cytometry. *Nat. Methods* **11**, 417–422 (2014).

ONLINE METHODS

Human breast cancer samples. Archival formalin-fixed, paraffin-embedded HER2-positive breast tumor samples were obtained for matched biopsies and tumors following neoadjuvant treatment for patients from Seoul National University Bundang Hospital. The institutional review boards of Seoul National University Bundang Hospital and the Dana-Farber/Harvard Cancer Center approved the protocol and waived the informed consent requirement. Samples were deidentified before analysis. Tumor histology and expression of standard biomarkers (estrogen receptor (ER), progesterone receptor (PR) and HER2) were evaluated at the time of diagnosis according to ASCO/CAP guidelines[50,51]. For the comparison of STAR-FISH and Sequenom MassARRAY, invasive ductal carcinoma (IDC) and adjacent ductal carcinoma *in situ* (DCIS) formalin-fixed, paraffin-embedded tissue slides were obtained following approval from the institutional review board at the Memorial Sloan Kettering Cancer Center; the informed consent requirement was waived. Tumor histology and marker analysis were performed as previously described[23].

Cell lines and HistoGel embedding. The breast cancer cell lines MDA-MB-231, T-47D, AU565 and BT-483 were obtained from the American Type Culture Collection (ATCC), and SUM-185PE cells were obtained from S. Ethier (University of Michigan). Cells were cultured in the media recommended by the provider. The identity of the cell lines was confirmed by short–tandem repeat (STR) analysis. Tests for mycoplasma contamination were performed regularly. For HistoGel embedding, BT-483 cells were fixed in 4% paraformaldehyde for 20 min, dehydrated in a series of increasing concentrations of ethanol and resuspended in 2 volumes of HistoGel (Thermo Scientific), prewarmed to 55 °C. Once solidified, the HistoGel was kept in 70% ethanol and processed into a paraffin block.

Xenograft assays. All animal procedures were approved by the Dana-Farber Cancer Institute Animal Care and Use Committee (ACUC) and followed US National Institutes of Health guidelines. Bilateral mammary fat pad injection of 1×10^6 cells resuspended in 50% Matrigel (BD Biosciences) per transplant were performed on 4- to 5-week-old female NCRNU-F mice (Taconic). Tumor volumes were monitored by biweekly caliper measurements until a volume of 1.2 cm^3 was reached. Tumors were then excised and processed into formalin-fixed, paraffin-embedded blocks. For xenograft assays with mixed cell lines, MDA-MB-231 and SUM-185PE cells expressing mCherry and GFP, respectively, were generated by lentiviral infection, as previously described[52]. Cells were collected, mixed at different ratios (total cell number of 2×10^6), mixed with 50% Matrigel and injected into the mammary fat pad of NCRNU-F mice. Tumors were removed when they reached 1 cm in diameter and cut into two equal pieces—one for formalin-fixed, paraffin-embedded processing and one for FACS analysis.

FACS for GFP- and mCherry-labeled cells. Tumor tissue was digested with 2 mg/ml collageanse I (Worthington Biochemical Corporation) and 2 mg/ml hyaluronidase (Sigma-Aldrich). Following dissociation, the sample was passed through a 40-µm cell strainer (BD Biosciences), washed in PBS with 0.5 mM EDTA and 5% BSA, and analyzed on a BD LSRFortessa analyzer. The gating for forward scatter and side scatter was set to exclude dead cells and doublets.

Immunofluorescence analyses. After deparaffininzation and rehydration, slides were subjected to antigen retrieval in citrate buffer (pH 6; Dako) for 20 min in a steamer. Blocking solution (10% FCS in PBST) was applied for 10 min. Incubation with primary antibody in PBS was held overnight at 4 °C in a moist chamber. Secondary antibody was applied for 45 min at room temperature. Samples were mounted with VectaShield HardSet Antifade Mounting Medium with DAPI (Vector Laboratories). Imaging was performed on a Leica SP5 confocal microscope. The antibodies used[52] included monoclonal antibody to GFP (sc-9996, mouse monoclonal IgG2a, Santa Cruz Biotechnology; 1:50 dilution), goat antibody to rabbit conjugated to Alexa Fluor 488 (Life Technologies; 1:100 dilution) and mouse monoclonal antibody to SMA (M085101, clone 1A4, mouse monoclonal IgG2a, Dako; 1:250 dilution).

STAR-FISH *in situ* PCR conditions. The first round of *in situ* PCR for the *PIK3CA* mutation encoding p.His1047Arg was performed with 2 mM $MgCl_2$, 200 µM dNTPs, 250 nM primers (for primer design, see the **Supplementary Note**) and 0.1 U/µl Platinum Taq Polymerase (Life Technologies) in 10× Platinum Taq Buffer (without $MgCl_2$; Life Technologies). A total of nine cycles were performed, in three steps of three cycles each with annealing temperatures at 45 °C, 52 °C and 58 °C. All cycling steps were 30 s long. The second round of PCR for the *PIK3CA* mutation encoding p.His1047Arg was performed with 3.5 mM $MgCl_2$, 200 µM dNTPs, 250 nM primers and 0.1 U/µl Platinum Taq Polymerase in 10× Platinum Taq Buffer (without $MgCl_2$). A total of 30 cycles were performed, 5 cycles with the annealing temperature at 45 °C, 5 cycles with the annealing temperature at 52 °C and 20 cycles with the annealing temperature at 58 °C. All cycling steps were 30 s long. The first round of PCR for the *PIK3CA* mutation encoding p.Glu542Lys was performed with 4 mM $MgCl_2$, 150 µM dNTPs, 250 nM primers and 0.1 U/µl Platinum Taq Polymerase in 10× Platinum Taq Buffer (without $MgCl_2$). A total of nine cycles were performed, with the annealing temperature at 56 °C; the cycling steps were 30 s long. The second round of PCR for the *PIK3CA* mutation encoding p.Glu542Lys was performed as for the *PIK3CA* mutation encoding p.His1047Arg, with 4 mM $MgCl_2$ and 150 µM dNTPs. For the *TP53* mutation encoding p.Arg175His, 2 mM $MgCl_2$ and 200 µM dNTPs were used in both PCR rounds. Because the amplicon resides in a GC-rich region, deoxy-7-deazaguanosine triphosphate (dc^7GTP) was added and a slowdown PCR program was used, as described before[53]. The second round of PCR was performed as for the *PIK3CA* mutation encoding p.His1047Arg.

STAR-FISH. Formalin-fixed, paraffin-embedded tissue sections (5 µm thick) on silylated glass slides were baked overnight at 70 °C, dewaxed in xylene (Leica Microsystems), washed in 100%, 70% and 50% ethanol (Leica Microsystems), rinsed with water and air dried for 1 h. After baking at 105 °C for 2 min, the samples were treated with 20 µg/ml proteinase K in PBS (Ambion) at 37 °C for 12 min (xenografts) or 18–20 min (human tumors). To increase the signal-to-noise ratio, the slides were then rinsed in water and treated with 100 µg/ml RNase in 2× SSC buffer (Fisher Scientific) for 1 h at 37 °C. Next, a 5-min wash in 5% Chelex beads (Bio-Rad) in water with agitation was applied and followed by two more washes with water. Excess water was drained, frame-seal incubation chambers (Bio-Rad) were applied to the slides, the master mix for the first round of PCR was pipetted on top of the tissue, the chambers were sealed and the slides were placed in the *in situ* PCR machine (Bio-Rad DNA Engine with Slide Tower). The first round of PCR was run for nine cycles. The frames were removed, excess remaining reagents were drained and new frames were applied before the addition of the master mix for the second round of PCR. The second round of PCR was run for 30 cycles. After removal of the frames, the slides were washed in water, dehydrated in increasing concentrations of ethanol (50%, 70%, 85% and 100%) and air dried. FISH probe mix, containing custom-designed probes recognizing wild-type and mutant PCR products (labeled with dFluorescein and TYE, respectively; Exiqon), *HER2* BAC probe (RP11-94L15; kindly provided by H. Russness and I. Rye; labeled with Spectrum Orange dUTP by Nick-Translation kit (Abbott Molecular)) and CEP17Aqua probe (Abbott Molecular), was then added to the slides, and coverslips were applied and sealed with rubber cement. Hybridization was performed for 7 min at 75 °C followed by overnight incubation at 37 °C in a humid chamber. The slides were then washed in 0.4× SSC with 0.3% NP-40 for 2 min at room temperature and 0.4× SSC with 0.3% NP-40 for 2 min at 74 °C followed by rinses in 2× SSC with 0.1% NP-40, 2× SSC and PBS. Nuclear counterstaining was performed by incubation for 10 min at room temperature with 1 µM To-Pro-3 in PBS (Molecular Probes, Life Technologies). After two additional washes in PBS and one wash in water, the slides were dried and mounted with VectaShield Mounting Medium (Vector Laboratories), covered with coverslips and stored overnight to 3 d at −20 °C.

Image acquisition and quantification of STAR-FISH signal. STAR-FISH images were acquired in *z* stacks (0.25 µm thick per slice, average of seven slices per image) with a Leica SP5X laser-scanning confocal microscope with a white-light laser and 63× Plan Apo objective. Image resolution was set at 1,024 × 1,024 pixels, and the scanning speed was set at 400 Hz. All images were acquired in sequential mode to avoid fluorophore crosstalk. For each sample, 3–5 images of different regions were collected to account for intratumoral

doi:10.1038/ng.3391

heterogeneity. Analysis of the images was conducted using ImageJ software. Maximum projection from the *z* stack was used to facilitate quantification of the FISH signal. Automated counting of STAR-FISH signal in each individual nucleus was performed with a custom macro in ImageJ (code available upon request). An outline was created for each nucleus, which was then applied as the region of interest for particle analysis for all STAR-FISH channels. As a result, for each image, a table was generated containing the cell index and measurements of the STAR-FISH particles found in each nucleus. The size of the nuclei was restricted to filter out stromal cells, which usually have smaller nuclei than tumor cells.

Droplet digital PCR. Tissue from three deparaffinized formalin-fixed, paraffin-embedded slides was scraped into an Eppendorf tube and resuspended in LowTE buffer with 1% SDS containing 10 µg/ml proteinase K and 10 µg/ml RNase. Samples were incubated at 56 °C for 48 h; proteinase K and RNase were added to final concentrations of 10 µg/ml every 12 h. DNA was extracted using TE-buffered phenol-chloroform (pH 8) (Fisher Scientific) according to the standard protocol. For control cell lines, MDA-MB-231 (*PIK3CA* wild type) and SUM-185PE (homozygous for *PIK3CA* mutation encoding p.His1047Arg), DNA was prepared in the same way, except for HCT116 cells (heterozygous for *PIK3CA* mutation encoding p.His1047Arg), for which a QIAamp DNA Mini kit (Qiagen) was used. PCR reactions (25 µl) that comprised ddPCR Supermix for Probes, custom TaqMan primer and probe mix (for primer and probe sequences, see **Supplementary Table 1**) and appropriate DNA template were prepared in a 96-well PCR plate and subsequently transferred to the sample wells of a digital droplet PCR cartridge. After Droplet Generator Oil (70 µl) was pipetted into the oil wells, the cartridge was loaded into the Droplet Generator. The emulsified droplets were then transferred to a new 96-well PCR plate, and DNA was amplified by PCR. The cycling conditions were as follows: 10 min at 95 °C followed by 40 cycles of a 2-step thermal profile of 15 s at 94 °C for denaturation and 60 s at 59 °C. The 96-well plate was then loaded onto and read by a QX100 Droplet Reader (Bio-Rad). Data analysis was performed using QuantaSoft software (v.1.6.6). The genomic populations of the *PIK3CA* alleles encoding histidine (wild type) and arginine (mutant) at codon 1047 in the template were determined by Poisson distribution fit. The assay was validated with cell line DNA (data not shown).

Sequenom MassARRAY. DCIS samples and their adjacent invasive breast carcinomas were microdissected with a sterile needle under a stereomicroscope and subjected to DNA extraction. DNA samples from DCIS and invasive breast carcinoma samples, when present, were subjected to Sequenom MassARRAY analysis to detect *PIK3CA* hotspot mutations as previously described[23,24]. The multiplexed assays were designed using Assay Design 3.1 Sequenom software, as previously reported[23]. In brief, amplification before PCR was performed using the same primers employed for Sequenom, before the iPLEX Gold genotyping assay. The purified primer extension reaction (7 nl) was loaded on the matrix pad of a SpectroCHIP (Sequenom) and measured by laser desorption/ionization time-of-flight mass spectrometry. The allelic fractions were estimated by calculating the ratio of the area of the raw spectra for the mutant allele to that for its wild-type counterpart[23,54].

Statistical and mathematical analyses. *Diversity index calculation.* For patient *i*, where $i = 1, 2, \ldots, 22$, denote the number of samples at diagnosis by n_{i1} and the number of samples obtained after the completion of treatment by n_{i2}. We had a total of $n_1 = 101$ samples at diagnosis and $n_2 = 82$ samples after treatment and a combined number of $n = n_1 + n_2 = 183$ samples. From the raw data, for each sample, we obtained the following numbers of cells identified by a particular mutation pattern: m_a cells with wild-type *PIK3CA* with neither *PIK3CA* mutation nor *HER2* amplification (WT), m_b cells with *PIK3CA* mutation without *HER2* amplification (MUT), m_c cells with *PIK3CA* mutation and *HER2* amplification (MUT + AMP), m_d cells with *HER2* amplification with neither *HER2* wild-type signal nor *PIK3CA* mutation (AMP) and m_e cells with *PIK3CA* wild-type signal without *PIK3CA* mutation but with *HER2* amplification (WT + AMP). We had a total of $m_a + m_b + m_c + m_d + m_e = m$ cells, for each *m* from the 183 samples at 2 time points. We also obtained $p_s = m_s/m$ for each cell type *s* from types {a,b,c,d,e}. Using these data, we then calculated an integrative Shannon index for each patient as follows where P_{ijts} is the proportion of the *s*th species in the *j*th sample for the *i*th patient at time point *t*:

$$H_{it} = -\prod_{j\in\{1,2,\ldots,i_t\}} H_{ijt} = -\prod_{j\in\{1,2,\ldots,i_t\}} \sum_{S\in\{a,b,c,d,e\}} p_{ijts} ln p_{ijts}$$

Analysis of changes in diversity. To make an inference on whether the diversity of cells within each patient changed significantly during treatment, we exploited a nonparametric bootstrap approach[55]. For sample *j* of patient *i* at time *t*, suppose that there are m_{ijt} cells. We then sampled a new set of m_{ijt} cells with replacement from those m_{ijt} cells and recalculated H_{it}^b for $b = 1, 2, \ldots, B$, where *b* indexes the bootstrap sample. In our analyses, we chose $B = 1{,}000$. Subsequently, the standard deviation from the bootstrapped integrative Shannon indices was calculated to generate 95% confidence intervals. If the confidence intervals of the pretreatment and post-treatment Shannon indices did not overlap, we deduced that the diversity of cell types within this patient changed significantly during treatment. The direction of change was subsequently determined by the sign of $H_{i2} - H_{i1}$.

Co-occurrence analyses of PIK3CA mutation and HER2 amplification. We then sought to investigate whether cells with *PIK3CA* mutation were more or less likely to contain *HER2* amplification as compared to cells with wild-type *PIK3CA*. To this end, we determined the following quantities for each sample: (i) the total number of cells in the sample, *n*; (ii) the number of cells with *PIK3CA* mutation, n_p; (iii) the number of cells with *HER2* amplification, n_h; and (iv) the number of cells with both *HER2* amplification and *PIK3CA* mutation, n_{hp}. If the two events are independent, then we should have $\text{Proportion}_{hp} \sim \text{Proportion}_h \text{Proportion}_p$. Thus, the binomial test was adopted to test the null hypothesis that *PIK3CA* mutation and *HER2* amplification emerge independently, where n_p/n is the background probability of *HER2* amplification, which is compared to a binomial distribution with n_{hp} realizations and n_h totals.

Inferring temporal ordering for PIK3CA mutation and HER2 amplification. We then sought to determine whether *PIK3CA* mutation or *HER2* amplification arose first within a cell. We considered that cells grow according to an exponential growth model. The numbers of cells with *PIK3CA* mutation or *HER2* amplification (assuming independence) over time was then modeled as follows:

$$n_p(t_p) = n_p(0)e^{(\lambda_p - \mu_p)t_p}$$

$$n_h(t_h) = n_h(0)e^{(\lambda_h - \mu_h)t_h}$$

The parameters λ_* and μ_* denote the birth and death rates of each cell type, respectively, with the subscript indicating either of the two cell types. We used the subscript p to denote parameters for cells carrying a *PIK3CA* point mutation and the subscript h to denote parameters for cells carrying a *HER2* amplification. To estimate λ_* and μ_*, we used previously published measurements obtained from a mouse model[42]. Using these data (**Fig. S2B** from Hanker *et al.*[42]), we found that the death rates for both cell types were lower than 0.1, and the estimates for λ_p and λ_h were around 0.9 and 0.75, respectively. Then, assuming that initially there is one cell of each type, the time it takes to reach n_p or n_h cells is given by:

$$t_p = \frac{\log n_p(t_p)}{\lambda_p - \mu_p}$$

$$t_h = \frac{\log n_h(t_h)}{\lambda_h - \mu_h}$$

The indicator $z = I(t_h < t_p)$ then provides us with the temporal order of the two types of mutations: if $z = 1$, then *HER2* amplification is the first event and, if otherwise, it is the second event. For each patient, we used the number of cells carrying *HER2* amplification at the pretreatment time point as $n_h(t_h)$ and the number of cells carrying a *PIK3CA* point mutation as $n_p(t_p)$. Because the birth rates and death rates were measured in a mouse model and these parameters might differ from the rates in human cells, sensitivity analyses were performed to investigate the robustness of the identified temporal order to perturbations in the parameter values. First, we changed the birth rate for *HER2*-amplified

cells to the following values: 0.5, 0.55, …, 0.9, in increments of 0.05. We found that the model using any of these values predicted that *HER2* amplification was the first event. Second, we changed the death rate for *HER2*-amplified cells to the following values: 0.06, 0.10, 0.14, 0.18 and 0.22. Similarly, we found that *HER2* amplification was the first event in all these scenarios. Thus, we conclude that *HER2* amplification is very likely the first event, followed by *PIK3CA* mutation, even taking into account the uncertainty in parameter estimation and differences in estimates between human and mouse cells. To perform a more detailed analysis of the evolutionary dynamics of the acquisition of these mutations, additional data from human cells are necessary.

Spatial analyses. We then sought to determine whether there was any spatial clustering of the cell types within samples. For each sample, we obtained a 1,024 × 1,024 pixel square image to display the spatial distribution of each measured cell. For each sample and each mutation type, we performed k-means clustering[43] with $k = 3$. We then calculated the ratio of between-cluster sums of squares versus the total sums of squares to quantify the randomness in localization for each mutation species. When this ratio is larger, $k = 3$ is sufficient to cluster the spatial data, whereas when this ratio is lower the spatial data might form smaller clusters and $k = 3$ is insufficient, with cells more sporadically distributed. Finally, we used the Wilcoxon rank-sum test to determine whether there was any significant difference in the distribution of this ratio between pretreatment and post-treatment samples.

50. Hammond, M.E. *et al.* American Society of Clinical Oncology/College of American Pathologists guideline recommendations for immunohistochemical testing of estrogen and progesterone receptors in breast cancer. *Arch. Pathol. Lab. Med.* **134**, 907–922 (2010).
51. Wolff, A.C. *et al.* Recommendations for human epidermal growth factor receptor 2 testing in breast cancer: American Society of Clinical Oncology/College of American Pathologists clinical practice guideline update. *Arch. Pathol. Lab. Med.* **138**, 241–256 (2014).
52. Marusyk, A. *et al.* Non-cell-autonomous driving of tumour growth supports sub-clonal heterogeneity. *Nature* **514**, 54–58 (2014).
53. Frey, U.H., Bachmann, H.S., Peters, J. & Siffert, W. PCR-amplification of GC-rich regions: 'slowdown PCR'. *Nat. Protoc.* **3**, 1312–1317 (2008).
54. Duprez, R. *et al.* Immunophenotypic and genomic characterization of papillary carcinomas of the breast. *J. Pathol.* **226**, 427–441 (2012).
55. Efron, B. & Tibshirani, R.J. *An Introduction to the Bootstrap* (Chapman & Hall, 1993).

doi:10.1038/ng.3391